JACS
JOURNAL OF THE AMERICAN CHEMICAL SOCIETY
Article
pubs.acs.org/JACS

Amine Oxidative N-Dealkylation via Cupric Hydroperoxide Cu-OOH Homolytic Cleavage Followed by Site-Specific Fenton Chemistry

Sunghee Kim,[†,§] Jake W. Ginsbach,[‡,§] Jung Yoon Lee,[†] Ryan L. Peterson,[†] Jeffrey J. Liu,[†] Maxime A. Siegler,[†] Amy A. Sarjeant,[†] Edward I. Solomon,*[,‡] and Kenneth D. Karlin*[,†]

[†]Department of Chemistry, Johns Hopkins University, Baltimore, Maryland 21218, United States
[‡]Department of Chemistry, Stanford University, Stanford, California 94305, United States

Supporting Information

ABSTRACT: Copper(II) hydroperoxide species are significant intermediates in processes such as fuel cells and (bio)chemical oxidations, all involving stepwise reduction of molecular oxygen. We previously reported a Cu^{II}-OOH species that performs oxidative N-dealkylation on a dibenzylamino group that is appended to the 6-position of a pyridyl donor of a tripodal tetradentate ligand. To obtain insights into the mechanism of this process, reaction kinetics and products were determined employing ligand substrates with various *para*-substituent dibenzyl pairs (-H,-H; -H,-Cl; -H,-OMe, and -Cl,-OMe), or with partially or fully deuterated dibenzyl N-$(CH_2Ph)_2$ moieties. A series of ligand–copper(II) bis-perchlorate complexes were synthesized, characterized, and the X-ray structures of the -H,-OMe analogue were determined. The corresponding metastable Cu^{II}-OOH species were generated by addition of H_2O_2/base in acetone at −90 °C. These convert ($t_{1/2} \approx 53$ s) to oxidatively N-dealkylated products, producing *para*-substituted benzaldehydes. Based on the experimental observations and supporting DFT calculations, a reaction mechanism involving dibenzylamine H-atom abstraction or electron-transfer oxidation by the Cu^{II}-OOH entity could be ruled out. It is concluded that the chemistry proceeds by rate limiting Cu-O homolytic cleavage of the Cu^{II}-(OOH) species, followed by site-specific copper Fenton chemistry. As a process of broad interest in copper as well as iron oxidative (bio)chemistries, a detailed computational analysis was performed, indicating that a Cu^{I}OOH species undergoes O–O homolytic cleavage to yield a hydroxyl radical and Cu^{II}OH rather than heterolytic cleavage to yield water and a Cu^{II}-$O^{\bullet-}$ species.

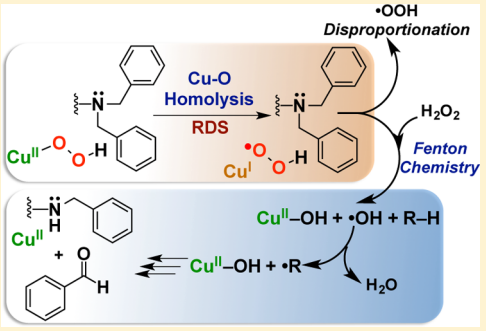

INTRODUCTION

Mononuclear copper species derived from reactions of ligand–Cu^{I} with O_2, such as Cu^{II}-superoxide, Cu^{II}-hydroperoxide, and copper-oxo {Cu^{III}=O ↔ Cu^{II}-$O^{\bullet-}$} species,[1] have all been considered as possible reactive intermediates formed during catalytic turnover in certain copper monooxygenases, including peptidylglycine-α-hydroxylating monooxygenase (PHM).[2] This enzyme possesses a "non-coupled" dicopper active site with two separated (~11 Å) copper ions: Cu_M, with His_2Met ligation where O_2 is activated for reaction with substrate, and Cu_H, an electron-transfer site with His_3 coordination.[2c,d] Recent enzymatic,[3] spectroscopic,[4] and theoretical investigations[4,5] indicate that a Cu^{II}-superoxide species (from Cu^{I}/O_2) initially attacks the substrate C–H bond in PHM. However, alternative reaction sequences[6] have been proposed, including substrate H-atom abstraction coming from a further downstream Cu^{II}-OOH[2a,7] or Cu^{II}-$O^{\bullet-}$[8] intermediates. As may be pertinent to PHM, other Cu enzymes,[2d] or synthetic and practical oxidation–oxygenation chemistries, it is critical to elucidate fundamental aspects of the formation, structural/spectroscopic, and reactivity characteristics of all these intermediates. Our research program includes such approaches, especially for Cu^{II}-$O_2^{\bullet-}$[1d,7,9] and Cu^{II}-$^{-}$OOH[6,10] complexes. Although a few well-characterized Cu^{II}-OOH complexes have been described,[1a,11] not a great deal is known about the intrinsic scope of their reactivity and reaction mechanism(s).

In a previous study,[10a] we showed that a Cu^{II}-OOH species can perform oxidative N-dealkylation reactions on a pyridyl (PY) ligand pendant dimethylamine (PY-NMe_2) moiety as substrate, leading to a product secondary amine (PY-NHMe) and formaldehyde deriving from the oxidized methyl group (Scheme 1). This reaction closely resembles the N-dealkylation chemistry occurring in PHM (Scheme 1).

For this system, a net H-atom abstraction mechanism was proposed, however, primarily on the basis of the observed kinetic isotope effect, KIE ≈ 2,[10a] which is low compared to what may be expected. Similar chemistry occurred when a dibenzylamine internal substrate [PY-N$(CH_2Ph)_2$] was present (Scheme 1).[6]

In this report, we describe experiments designed to more deeply probe the mechanism of these reactions. A combination of experimental results and density functional theory (DFT) calculations have led us to propose a new reaction mechanism that is potentially applicable to many chemical systems and possibly situations where metal hydroperoxo species form in

Received: August 16, 2014
Published: February 23, 2015

DOI: 10.1021/ja508371q
J. Am. Chem. Soc. 2015, 137, 2867–2874

Scheme 1

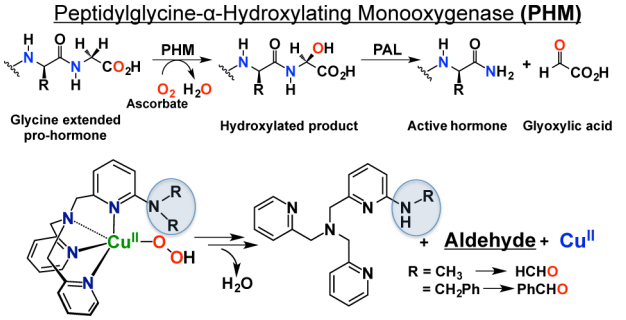

biology. For the net hydroxylation of the dibenzylamine C−H substrate (i.e., methylene group), a rate-determining homolytic cleavage of the Cu^{II}−O bond in the Cu^{II}-hydroperoxide occurs first. This is followed by a site specific copper Fenton chemical reaction between the resulting Cu^{I} species and a second equivalent of hydrogen peroxide, producing a hydroxyl radical that is responsible for the C−H activation.

EXPERIMENTAL SECTION

General. All materials used were commercially available analytical grade from Sigma-Aldrich, and TCI. Acetone was distilled under an inert atmosphere over anhydrous $CaSO_4$ and degassed with argon prior to use. Diethyl ether was used after being passed through a 60 cm long column of activated alumina (Innovative Technologies) under argon. Benzaldehyde and triethylamine were distilled under vacuum prior to use. $(Ph_3P{=}O)_2{\cdot}H_2O_2$ was synthesized according to literature protocols, and its identity and purity were verified by ^{1}H NMR and elemental analysis.[12] Synthesis and manipulations of copper salts were performed according to standard Schlenk techniques or in an MBraun glovebox (with O_2 and H_2O levels below 1 ppm). Carbon monoxide (CO) gas was obtained from Airgas and passed through an oxygen and moisture scrubbing column.

Instrumentation. UV−vis spectra were recorded with an HP model 8453A diode array spectrophotometer equipped with a liquid nitrogen chilled Unisoku USP-203-A cryostat; kinetic measurements were maintained at −90 °C ± 1%. NMR spectroscopy was performed on Bruker 300 and 400 MHz instruments with spectra calibrated to either internal tetramethylsilane (TMS) standard or to residual protio solvent. EPR measurements were performed on an X-Band Bruker EMX CW EPR controlled with a Bruker ER 041 XG microwave bridge operating at the X-band (~9 GHz). GC was performed on an Agilent 6890 gas chromatograph fitted with a HP-5 (5%-phenyl)-methylpolysiloxane capillary column (30 m × 0.32 mm × 0.25 mm) and equipped with a flame-ionization detector. The GC-FID response factors for benzaldehydes were prepared vs dodecane as an internal standard. ESI mass spectra were acquired using a Finnigan LCQDeca ion-trap mass spectrometer equipped with an electrospray ionization source (Thermo Finnigan, San Jose, CA). GC-MS experiments were carried out and recorded using a Shimadzu GC-17A/GCMS0QP5050 gas chromatograph/mass spectrometer. X-ray diffraction was performed at the X-ray diffraction facility at the Johns Hopkins University. The X-ray intensity data were measured on an Oxford Diffraction Xcalibur3 system equipped with a graphite monochromator and an Enhance (Mo) X-ray Source (λ = 0.71073 Å) operated at 2 kW power (50 kV, 40 mA) and a CCD detector. The frames were integrated with the Oxford Diffraction *CrysAlisRED* software package.

Synthesis of Ligands. *DB ($L^{H,H}$).* BrTMPA (2.1 g, 5.69 mmol) and dibenzylamine (6 g, 30.41 mmol) were placed in a high-pressure tube (Ace pressure tube, Aldrich Z18, 106-111) and dissolved in 3 mL of toluene/12 mL of water with 0.1 g of NaOH (Scheme 2). The resulting mixture was stirred at 160 °C for 7 days and then cooled to room temperature. The resulting mixture was extracted with CH_2Cl_2 several times. The combined organic layers were dried over anhydrous $MgSO_4$ and filtered, and the volatile components were removed by

Scheme 2

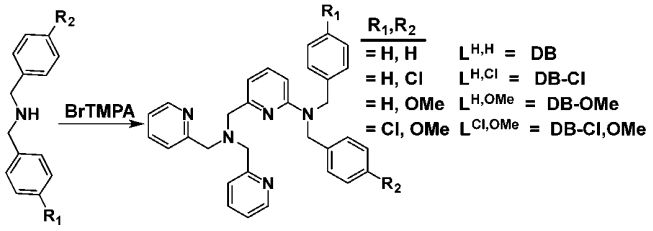

rotary evaporation, yielding a pale yellow oil. The resulting yellow oil was purified by column chromatography (silica gel, 100% ethyl acetate, R_f = 0.36). The product fraction was collected, and the solvent was removed under reduced pressure to afford the pale yellow oil, DB (1.22 g, 77% yield).[10a] ^{1}H NMR (400 MHz, $CDCl_3$): δ 8.59 (d, 2H), 7.63 (d, 2H), 7.54 (t, 2H), 7.37−7.11 (m, 8H), 7.10 (t, 2H), 6.84 (d, 2H), 6.76 (d, 1H), 6.33 (d, 1H), 4.81 (s, 4H, $2CH_2Ph$), 3.90 (s, 4H, $2CH_2Py$), 3.70 (s, 2H, CH_2Py). ESI-MS, m/z: 508.4 ($M + Na^+$), 486.3 ($M + H^+$) in MeOH at room temperature.

DB-OMe ($L^{H,OMe}$). ^{1}H NMR (400 MHz, $CDCl_3$): δ 8.60 (d, 2H), 7.63 (d, 2H), 7.54 (t, 2H), 7.35−7.21 (m, 10H), 7.10 (t, 2H), 6.76 (d, 1H), 6.33 (d, 1H), 4.81 (s, 4H, $2CH_2Ph$), 3.90 (s, 4H, $2CH_2Py$), 3.70 (s, 2H, CH_2Py). ESI-MS, m/z: 538.4 ($M + Na^+$), 516.3 ($M + H^+$) in MeOH at room temperature.

DB-Cl ($L^{H,Cl}$). ^{1}H NMR (400 MHz, $CDCl_3$): δ 8.59 (d, 2H), 7.63 (d, 2H), 7.54 (t, 2H), 7.35−7.21 (m, 10H), 7.10 (t, 2H), 6.76 (d, 1H), 6.33 (d, 1H), 4.80 (s, 2H, CH_2Ph), 4.76 (s, 2H, CH_2Ph), 3.89 (s, 4H, $2CH_2Py$), 3.70 (s, 2H, CH_2Py). ESI-MS, m/z: 542.2 ($M + Na^+$), 520.2 ($M + H^+$) in MeOH at room temperature.

DB-Cl,OMe ($L^{Cl,OMe}$). ^{1}H NMR (400 MHz, $CDCl_3$): δ 8.56 (d, 2H), 7.63 (d, 2H), 7.54 (t, 2H), 7.40−7.10 (m, 9H), 6.82 (d, 2H), 6.75 (d, 1H), 6.32 (d, 1H), 4.75 (s, 4H, $2CH_2Ph$), 3.90 (s, 4H, $2CH_2Py$), 3.80 (s, 3H), 3.70 (s, 2H, CH_2Py). ESI-MS, m/z: 572.5 ($M + Na^+$) in MeOH at room temperature.

Deuterated Benzaldehyde. *N,N*-Dimethylformamide-d_7 (1.03 g, 12.85 mmol) was placed in a two-neck flask in 50 mL of THF at −80 °C (Scheme 3). Next, 1.8 M phenyllithium solution (6.5 mL, 11.68

Scheme 3

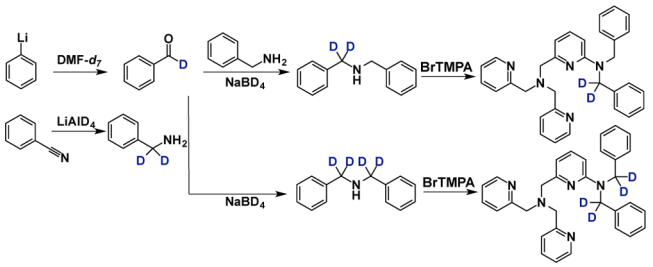

mmol) was slowly added to the solution at −80 °C. After being stirred for 1 h, the mixture solution was warmed up to room temperature. All solvents were removed by a rotary vacuum, affording a pale yellow oil. This resulting yellow oil was purified by column chromatography (silica gel, ethyl acetate:hexane = 1:6), and this material was used in the next step without further purification (see Partially Deuterated Dibenzyl Amine-d_2 below).

Deuterated Benzyl Amine. A 250 mL two-necked, round-bottomed flask was charged with lithium aluminum deuteride, 98 atom % D (Aldrich, $LiAlD_4$; 5.1 g 121.66 mmol) (Scheme 3).[13] The flask was fitted with a condenser and a septum and thoroughly purged with a steady stream of Ar. After 5 min, 60 mL of anhydrous diethyl ether was added via a syringe. The homogeneous solution was cooled in an ice bath to 0 °C. Benzonitrile (5.0 g, 48.49 mmol) in 10 mL of diethyl ether was slowly transferred via a syringe to the mixture over 10 min. After vigorous H_2 gas evolution ceased, the mixture solution was allowed to warm to ambient temperature and then refluxed overnight

DOI: 10.1021/ja508371q
J. Am. Chem. Soc. 2015, 137, 2867−2874

at 80 °C. The solution was cooled to room temperature, diluted with 65 mL of diethyl ether, cooled to 0 °C, and quenched by the successive dropwise addition of 3.8 mL of 10% NaOH solution and 11.4 mL of water. The colorless precipitate was vacuum filtered through Celite, and the filter cake was washed with diethyl ether (3 × 20 mL). The combined filtrate was concentrated to give a pale yellow oil. This resulting yellow oil was purified by column chromatography (silica gel, 100% ethyl acetate, R_f = 0.38), yielding a pale oil (4.6 g, 87% yield). ^{1}H NMR (400 MHz, $CDCl_3$): δ 7.40−7.23 (m, 5H).

Partially Deuterated Dibenzyl Amine-d_2. Deuterated benzaldehyde (4.2 g, 48.58 mmol) and benzylamine (4.2 g 58.808 mmol) were placed in 70 mL of EtOH in a 250 mL round-bottom flask, and then the mixture solution was stirred for 4 h under Ar to form an imine intermediate (Scheme 3). This intermediate imine can then be isolated and reduced with a suitable reducing agent, deuterated sodium borohydride. Deuterated sodium borohydride, 98 atom % D (Aldrich, $NaBD_4$; 3.3 g, 78.84 mmol), was slowly added to the solution and stirred for 30 min at room temperature. To quench excess $NaBD_4$, 20 mL of MeOH was slowly added at 0 °C, and then all solvents were removed by rotary evaporation. The resulting crude product was dissolved in 100 mL of CH_2Cl_2 and washed two times with a saturated Na_2CO_3 solution. After drying over anhydrous $MgSO_4$, the solution was filtered and removed by rotary evaporation. The resulting yellow oil was purified by column chromatography (silica gel, 20% ethyl acetate with hexane, R_f = 0.67) yielding a pale oil (7.5 g, 96% yield). ^{1}H NMR (400 MHz, $CDCl_3$): δ 7.40−7.23 (m, 10H), 3.80 (s, 2H). ESI-MS, m/z: 200.1 (L + H$^+$) in MeOH at room temperature.

Fully Deuterated Dibenzyl Amine-d_4. Deuterated benzaldehyde (5.2 g, 47.634 mmol) and deuterated benzylamine (6.3 g, 58.808 mmol) were placed in 70 mL of EtOH in a 250 mL round-bottom flask, and then the mixture solution was stirred for 4 h under Ar. Deuterated sodium borohydride, 98 atom % D (Aldrich, $NaBD_4$; 2 g, 47.78 mmol), was slowly added to the solution at 0 °C. To quench excess $NaBD_4$, 20 mL of MeOH was added, and then all solvents were removed by using reduced pressure. The resulting crude product was dissolved in 100 mL of CH_2Cl_2 and washed two times with a saturated Na_2CO_3 solution. After drying over anhydrous $MgSO_4$, the solution was filtered and removed by rotary evaporation. The resulting yellow oil was purified by column chromatography (silica gel, 20% ethyl acetate with hexane, R_f = 0.67), yielding a pale oil (7.5 g, 97% yield). ^{1}H NMR (400 MHz, $CDCl_3$): δ 7.35−7.26 (m, 10H), 2.18 (s, 1H). ESI-MS, m/z: 201.6 (L) in MeOH at room temperature.

DB-d_2 (d_2-$L^{H,H}$). ^{1}H NMR (400 MHz, $CDCl_3$): δ 8.59 (d, 2H), 7.63 (d, 2H), 7.54 (t, 2H), 7.37−7.11 (m, H), 7.10 (t, 2H), 6.76 (d, 1H), 6.33 (d, 1H), 4.81 (s, 2H, CH_2Ph), 3.90 (s, 4H, 2CH_2Py), 3.70 (s, 2H, CH_2Py). ESI-MS, m/z: 510.5 (L + Na$^+$), 488.5 (L + H$^+$) in MeOH at room temperature.

DB-d_4 (d_4-$L^{H,H}$). ESI-MS, m/z: 490.5 (L + H$^+$) in MeOH at room temperature.

Synthesis of Copper(II) Complexes. *[(DB)$Cu^{II}(H_2O)(OClO_3)$]-(ClO_4), $\mathbf{1}^{H,H}$.* The synthesis and characterization of the DB copper complex was recently reported. DB ligand (430 mg, 0.886 mmol) was treated with $Cu^{II}(ClO_4)_2\cdot 6H_2O$ (328 mg, 0.886 mmol) in acetone (20 mL) and stirred for 10 min at room temperature. The mixture complex was precipitated as a blue solid upon the addition of diethyl ether (120 mL). The supernatant was decanted, and the resulting crystalline solid was washed two times with diethyl ether and dried under reduced vacuum to afford a blue solid. The blue solid was recrystallized twice from acetone/diethyl ether. After vacuum-drying, the blue crystals weighed 587 mg (87% yield). Elemental analysis ($C_{35}H_{39}Cl_2CuN_5O_{10}$), calculated: C (51.01), H (4.77), N (8.50); found: C (50.95), H (4.66), N (8.42). ESI-MS: m/z = 548.5, corresponding to [(DB)Cu^I]$^+$ in acetone at room temperature (Figure S1). EPR spectrum, X-band (ν = 9.186 GHz) spectrometer in acetone at 70 K: $g_\parallel$ = 2.273, $g\perp$ = 2.048, $A_\parallel$ = 173 G.

[(DB-Cl)$Cu^{II}(CH_3COCH_3)$](ClO_4)$_2$, $\mathbf{1}^{H,Cl}$. Elemental analysis ($C_{35}H_{36}Cl_3CuN_5O_9$), calculated: C (50.01), H (4.32), N (8.33); found: C (50.17), H (4.52), N (8.32). ESI-MS: m/z = 582.5, corresponding to [(DB-Cl)Cu^I]$^+$ in acetone at room temperature. EPR spectrum, X-band (ν = 9.186 GHz) spectrometer in acetone at 70 K: $g_\parallel$ = 2.270, $g\perp$ = 2.043, $A_\parallel$ = 172 G.

[(DB-OMe)$Cu^{II}(OClO_3)CH_3COCH_3$)]($ClO_4$), $\mathbf{1}^{H,OMe}$. Single crystals of a [(DB-OMe)Cu^{II}(CH_3COCH_3)]$^{2+}$, $\mathbf{1}^{H,OMe}$ complex were obtained by vapor diffusion of diethyl ether into a solution of the copper complex in acetone. Elemental analysis ($C_{36}H_{39}Cl_2CuN_5O_{10}$), calculated: C (51.71), H (4.70), N (8.38); found: C (51.68), H (4.86), N (8.37). ESI-MS: m/z = 578.5, corresponding to [(DB-OMe)Cu^I]$^+$ in acetone at room temperature. EPR spectrum, X-band (ν = 9.186 GHz) spectrometer in acetone at 77 K: $g_\parallel$ = 2.277, $g\perp$ = 2.049, $A_\parallel$ = 175G.

[(DB-Cl-OMe)$Cu^{II}(CH_3COCH_3)$](ClO_4)$_2$, $\mathbf{1}^{Cl,OMe}$. Elemental analysis ($C_{36}H_{38}Cl_3CuN_5O_{10}$), calculated: C (49.66), H (4.40), N (8.04); found: C (49.35), H (4.45), N (7.79). ESI-MS: m/z = 612.5, corresponding to [(DB-Cl-OMe)Cu^I]$^+$ in acetone at room temperature. EPR spectrum, X-band (ν = 9.186 GHz) spectrometer in acetone at 70 K: $g_\parallel$ = 2.272, $g\perp$ = 2.044, $A_\parallel$ = 176 G.

[(d_2-$L^{H,H}$)$Cu^{II}(H_2O)$)](ClO_4)$_2$. ESI-MS: m/z = 550.5, corresponding to [d_2-($L^{H,H}$)Cu^I]$^+$ in acetone at room temperature (Figure S2). EPR spectrum, X-band (ν = 9.186 GHz) spectrometer in acetone at 70 K: $g_\parallel$ = 2.270, $g\perp$ = 2.043, $A_\parallel$ = 175 G (Figure S3).

[(d_4-$L^{H,H}$)$Cu^{II}(H_2O)$)](ClO_4)$_2$. ESI-MS: m/z = 552.5, corresponding to [(d_4-$L^{H,H}$)Cu^I]$^+$ in acetone at room temperature (Figure S2). EPR spectrum, X-band (ν = 9.186 GHz) spectrometer in acetone at 70 K: $g_\parallel$ = 2.270, $g\perp$ = 2.043, $A_\parallel$ = 172 G (Figure S3).

DFT Calculations. Calculations on the copper hydroperoxo complex supported by $\mathbf{L}^{H,H}$ were performed with the B3LYP functional and a TZVP basis set on the Cu-OOH fragment and the coordinating nitrogen atoms and SV on all other atoms as implemented in Gaussian 09.[14] A TZVP basis set was utilized for an additional equivalent of H_2O_2 and the nitrogen atom of NEt_3 (SV on all of the other atoms). Optimizations were performed in acetone with the polarizable continuum model on an ultrafine integration grid. Spin contamination was accounted for as described in the Supporting Information. Analytical frequency calculations were performed on all stationary points, and thermal corrections to the Gibbs free energy were determined at −90 °C. Transition states were connected to the corresponding products and reactants by optimizing from the transition-state geometry, slightly distorted along the computed imaginary frequency or with an intrinsic reaction coordinate.[11] Calculations on the [(TMG_3tren)Cu^{II}-OOH]$^+$ system (TMG_3tren = (1,1,1-tris[2-[N^2-(1,1,3,3-tetramethylguanidino)]ethyl]amine))) were performed as described previously[15] with Gaussian 03.[16]

RESULTS AND DISCUSSION

Mononuclear copper(II) complexes [($L^{X1,X2}$)Cu^{II}(Y)](ClO_4)$_2$ ($\mathbf{1}^{X1,X2}$) (Y = H_2O, acetone) were generated, isolated, and purified by reacting the various ligands (Scheme 4; X = Cl, H, or OMe) with Cu(ClO_4)$_2\cdot 6H_2O$ in acetone, precipitating solid products with Et_2O, and recrystallizing.[17] An X-ray crystallographically derived structural diagram for $\mathbf{1}^{H,OMe}$ is shown in Figure 1, along with spectroscopic data.[17]

Scheme 4

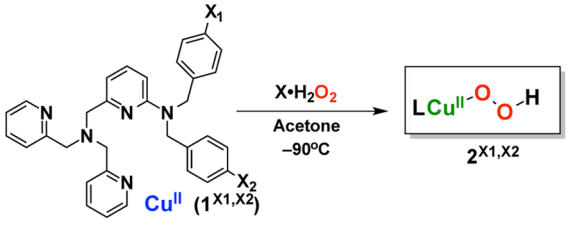

Cupric hydroperoxo complexes $\mathbf{2}^{X1,X2}$ were obtained at −90 °C in acetone by reacting Cu^{II} precursors $\mathbf{1}^{X1,X2}$ with 10 equiv of H_2O_2 or X·H_2O_2, X = urea, $(Ph_3P{=}O)_2$, in the presence of Et_3N (2 equiv) under Ar (Scheme 4). Under these conditions, a bright green product, [($L^{H,H}$)Cu^{II}-OOH]$^+$ ($\mathbf{2}^{H,H}$), forms,

DOI: 10.1021/ja508371q
J. Am. Chem. Soc. 2015, 137, 2867−2874

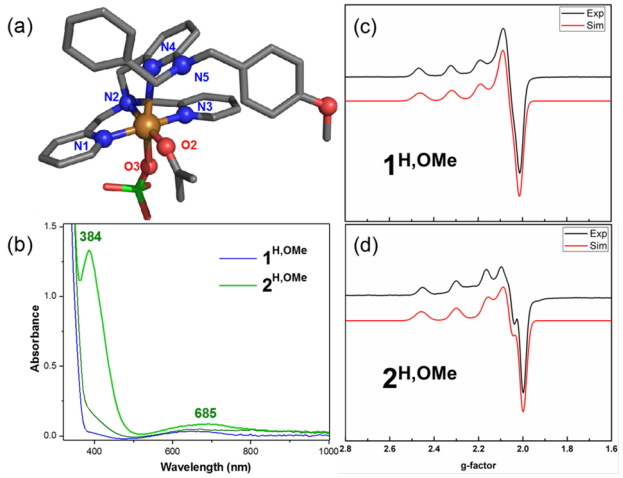

Figure 1. (a) X-ray crystal structure of $[(L^{H,OMe})Cu^{II}(OClO_3)(CH_3COCH_3)]^+$ ($\mathbf{1}^{H,OMe}$), revealing Cu(II) distorted octahedral coordination with three equatorial N and one $O_{(acetone)}$ donors (Cu−ligand =1.984 $Å_{(ave.)}$) and two elongated axial ligands, one pyridyl group (Cu−Npy =2.698(2) Å), and a perchlorate O atom (Cu−O = 2.492(2) Å).[17] (b) UV−vis spectrum of $\mathbf{1}^{H,OMe}$ (λ_{max} = 630 nm) and Cu^{II}-OOH complex $\mathbf{2}^{H,OMe}$. (c) EPR spectrum and simulated plot (red) of $\mathbf{1}^{H,OMe}$ (2 mM, $g_{\|}$ = 2.205, $A_{\|}$ = 206 G, $g\perp$ = 2.003). (d) EPR spectrum and simulated plot (red) of $\mathbf{2}^{H,OMe}$ (2 mM, $g_{\|}$ = 2.227, $A_{\|}$ = 205 G, $g\perp$ = 2.044); X-band (ν = 9.186 GHz) in acetone at 77 K.

possessing a LMCT band at 384 nm (ε = 2200 M^{-1} cm^{-1}) with a d−d band at 685 nm (ε = 150 M^{-1} cm^{-1}); similar UV−vis features are obtained for the other $[(L^{X1,X2})Cu^{II}$-OOH$]^+$ complexes, including $\mathbf{2}^{H,OMe}$ (Figure 1).[17] The g and A values obtained from EPR spectroscopy on the $[(L^{X1,X2})Cu^{II}$-OOH$]^+$ ($\mathbf{2}^{X1,X2}$) series are all similar, but distinguishable from the precursor copper(II) complexes $[(L^{X1,X2})Cu^{II}(Y)]^{2+}$ ($\mathbf{1}^{X1,X2}$) (see Figure 1). Integration of the EPR intensity of $\mathbf{1}^{X1,X2}$ and $\mathbf{2}^{X1,X2}$ indicates that $\mathbf{2}^{X1,X2}$ is formed in ∼80% yield under these conditions.

The hydroperoxo-copper(II) complexes $[(L^{X,X})Cu^{II}$-OOH$]^+$ ($\mathbf{2}^{X1,X2}$) (Scheme 5) are metastable, and in all cases, biomimetic oxidative N-dealkylation occurs, similar to the enzyme PHM (Scheme 1).[2] The rate of the reaction was monitored by the loss in the ∼384 nm band, which decayed in a first-order process at similar rates for all of the complexes in Scheme 5, k_{decay} = (4.17 ± 0.14) × 10^{-2} s^{-1} for $[(L^{H,H})Cu^{II}$-OOH$]^+$ (0.3 mM).[17] These results were initially surprising since the rate of

Scheme 5

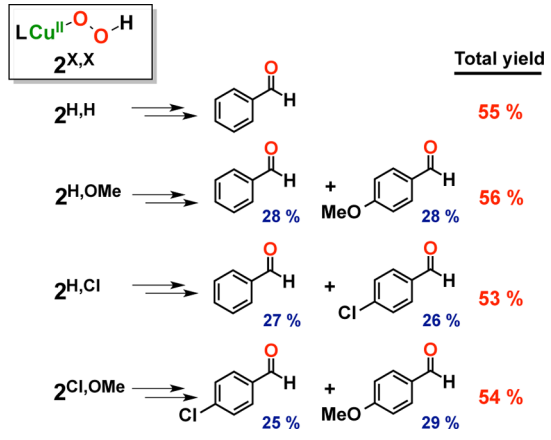

benzylic H-atom abstraction has been shown to depend on the *para*-substituent in other systems.[18] Hence, further studies were undertaken to test whether various *p*-benzyl (i.e., aryl) substituents in the hydroperoxo complexes $\mathbf{2}^{X1,X2}$ would lead to different yields of aldehyde products.

The overall and relative yields of benzaldehyde (Scheme 5) were quantified by GC analysis from samples taken directly from reaction solutions at −80 °C after 30 min. Complementary yields of secondary amines, i.e., the initial ligand with a lost benzylic arm, were obtained following reaction solution workup using $Na_2EDTA_{(aq)}$ or $NH_4OH_{(aq)}$ to demetallate the copper, followed by extraction of organics into CH_2Cl_2, and subsequent product analysis by NMR spectroscopy and ESI-MS (Scheme 6). The remainder of the ligand was unreacted $L^{X1,X2}$, indicating good mass balance for these reactions.[17]

Scheme 6

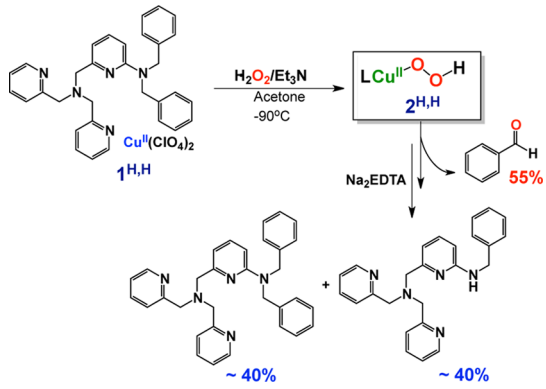

These results indicate that there is no discrimination for attack of the reactive species at the benzylic methylene substrate position, whether the aryl ring is electron rich (X = OMe) vs electron poor (X = Cl) since equal yields (average of three trials) of substituted benzyaldehydes are obtained. Even for the case of $\mathbf{2}^{Cl,OMe}$, equal amounts of *p*-chloro and *p*-methoxy benzyldehydes are obtained, Scheme 5. The lack of a substituent effect strongly implies that attack by whatever oxidant is involved does not include substrate methylene group H-atom transfer or hydride abstraction. Cu^{II}-OOH electron-transfer oxidation of the amine is also unlikely, *vide infra*.

Further insight comes from comparing the reactivity of the parent ligand ($L^{H,H}$ with its $-N(CH_2Ph)_2$ substrate) to a ligand with fully deuterated benzylic C−D bonds (d_4-$L^{H,H}$ with $-N(CD_2Ph)_2$) (Scheme 7). Kinetic interrogation of the

Scheme 7

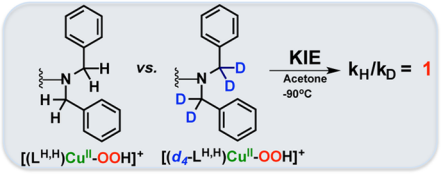

decomposition rates of $[(L^{H,H})Cu^{II}$-OOH$]^+$ vs $[(d_4$-$L^{H,H})$-Cu^{II}-OOH$]^+$ reveals that the KIE = k_H/k_D = 1.0 ± 0.1. We also examined products found from competitive internal ligand oxidation chemistry with the copper hydroperoxy complex of d_2-$L^{H,H}$ with $-N(CD_2Ph)(CH_2Ph)$ (Scheme 8). Again the KIE

DOI: 10.1021/ja508371q
J. Am. Chem. Soc. 2015, 137, 2867−2874

= 1.0 ± 0.1, based on the observation of equal yields of benzaldehyde and deuterated benzaldehyde.

Scheme 8

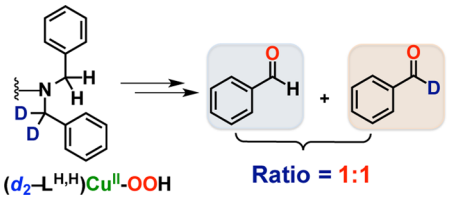

These results point to the fact that, in the rate-determining step, the Cu^{II}-OOH moiety decays/transforms to something more reactive, which leads to the oxidative N-dealkylation chemistry observed. This hypothesis is in agreement with past computational studies[4,5,19] that have indicated that H-atom abstraction by a Cu^{II}-OOH species is an unfavorable process. However, Poater and Cavallo have suggested that the distal oxygen of the Cu^{II}-OOH species, supported by the related tripodal tetradentate N_4 TMG_3tren ligand, directly abstracts a H-atom from the guanidinium methyl group ($\Delta G^{\ddagger}$ = 22 kcal/mol).[15] Given these disagreements, we computed the barrier for H-atom abstraction by the distal oxygen in $\mathbf{2}^{H,H}$ (Scheme 9,

Scheme 9

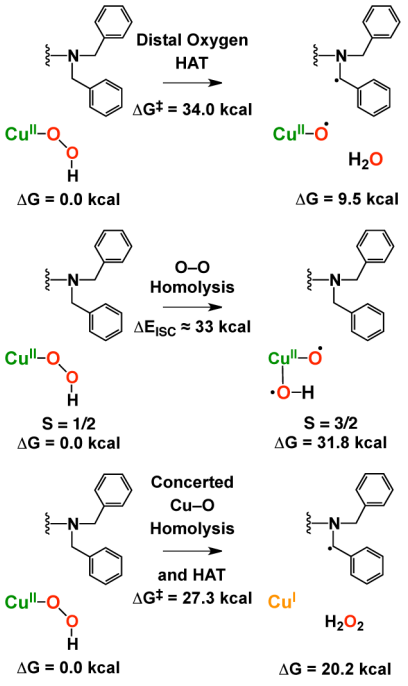

top). We calculated a large barrier for this mechanism ($\Delta G^{\ddagger}$ = 34.0 kcal/mol) and would expect to observe a large, normal KIE on the decay of the Cu^{II}-OOH species; however, this is inconsistent with the experimental results.

To determine the large discrepancy between the calculated barriers in these two systems, we reexamined the reported[15] calculations on the TMG_3tren system. We find that the 22 kcal/mol transition state for the H-atom abstraction by the Cu^{II}OOH does not connect on an intrinsic reaction coordinate (Figures S19 and S20) to the Cu^{II}-OOH intermediate. Rather, this transition state is best described as the reaction of a hydroxyl radical with the guanidinium H-atom (Scheme 10,

Scheme 10

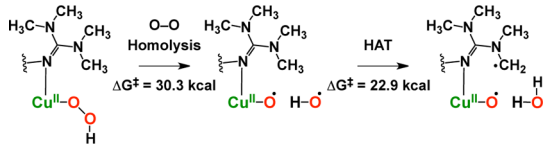

second step). To form this hydroxyl radical, the Cu^{II}-OOH must first undergo homolytic cleavage of the O–O bond, a process with a barrier of $\Delta G^{\ddagger}$ = 30.3 kcal in the TMG_3tren system.[17] Computing the barrier of O–O bond homolysis in the present system is complicated by the presence of an open, axial coordination site that leads to coordination of the hydroxyl radical produced (Scheme 9, middle). The quartet spin state is predicted to be lower in energy than the doublet state and the energy of the intersystem crossing (ΔE_{ISC}) is ∼33 kcal/mol, computed from the O–O potential energy surface (Figure S15). This barrier is inconsistent with the experimental rate (1.32×10^{-2} s^{-1}, see above) that predicts $\Delta G^{\ddagger} \approx 12$ kcal/mol at −90 °C. Hence these calculations predict that both mechanisms, the direct H-atom abstraction by the distal oxygen (Scheme 9, top) and the homolytic O–O bond cleavage (Scheme 9, middle), are inconsistent with the experimental findings.

We alternatively hypothesized that the observed products could result from rate-limiting Cu-OOH homolysis to give a Cu^{I} complex and a hydroperoxyl radical (•OOH). Such a reaction has been described,[20] and is consistent with the previously reported one-electron reduction of a Cu^{II} complex by hydrogen peroxide.[11c] This reaction is also favored by poorly donating ligands which stabilize the lower-valent Cu^{I} oxidation state. A reaction coordinate for the concerted Cu^{II}-OOH homolysis coupled to H-atom abstraction by the proximal oxygen yields an unfavorable activation barrier ($\Delta G^{\ddagger}$ = 27.3 kcal/mol) and is inconsistent with an isotope effect of 1 (Scheme 9, bottom). However, the calculated barrier for the homolytic cleavage of the Cu^{II}-OOH bond is equivalent to the bond dissociation energy (Figure S16) and energetically accessible (ΔG = 14.8 kcal/mol, Scheme 11). Hence, DFT calculations suggest that the most favorable decay pathway of the Cu^{II}-OOH intermediate produces a Cu^{I} complex and a hydroperoxyl radical.

The proposed homolytic cleavage of the Cu^{II}-OOH bond is also supported by the following observation. Bubbling carbon monoxide (CO) into a solution of $[(L^{H,H})Cu^{II}\text{-OOH}]^{+}$ ($\mathbf{2}^{H,H}$) at −90 °C causes the solution to change from light green (due to $\mathbf{2}^{H,H}$) to colorless (that being typical of such ligand–Cu^{I}–CO complexes)[21] and a much lower yield of benzaldehyde (∼19% compared to the usual ≥50%) is produced, an observation that may be explained by CO trapping the lower-valent Cu^{I} generated from Cu^{II}-OOH homolysis.

After the Cu^{II}-OOH bond has been cleaved, we hypothesized that the dibenzylamine containing C–H bond could be activated via a number of potential mechanisms to lead to the observed products (Scheme 11). Initially, we considered C–H abstraction by the free hydroperoxyl radical, but the computed barrier for this process is unfavorable ($\Delta G^{\ddagger}$ = 31.7 kcal/mol, Scheme 11, middle). These calculations suggest that this radical is not sufficiently reactive to activate the substrate C–H bond, likely due to the formation of a relatively weak O–H bond (88 kcal/mol) compared to the strong O–H bond of water (119 kcal/mol).[22] Another possibility involves the

DOI: 10.1021/ja508371q
J. Am. Chem. Soc. 2015, 137, 2867–2874

Scheme 11

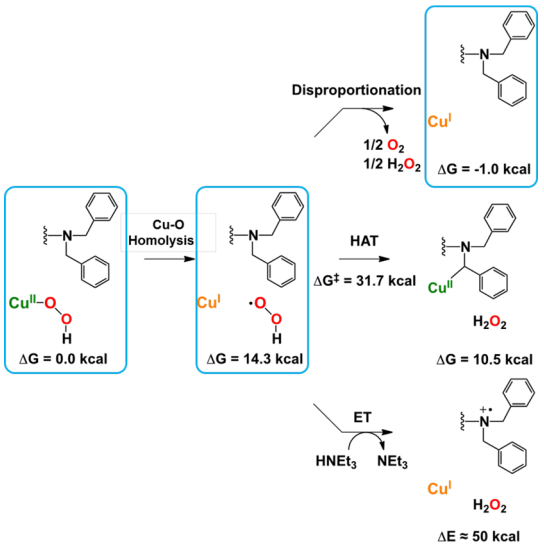

Scheme 12

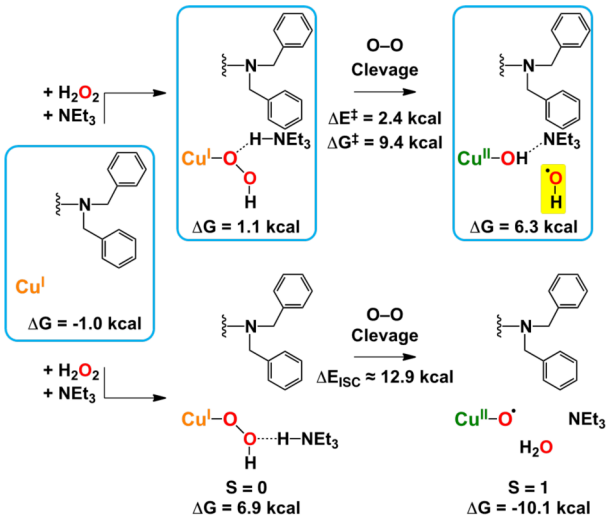

oxidation of the tertiary amine via electron transfer to the $^{\bullet}$OOH species to produce an ammonium radical cation (Scheme 11, bottom). However, DFT calculations suggest that the most favorable one electron oxidation of the Cu^{I} species gives the Cu^{II} complex, with the Cu^{I} ammonium radical cation being significantly higher in energy.[17] These computational results are consistent with experimental cyclic voltammetry data that observe a single, copper-based redox feature at −280 mV vs Ag^{+}/Ag° for all of the $\mathbf{1}^{X1,X2}$ cupric complexes (Figure S5).

This led us to consider disproportionation of the hydroperoxyl radical (Scheme 11, top) and that the observed C−H activation could be due to a subsequent reaction of the Cu^{I} complex. DFT calculations suggest that this disproportionation reaction is favorable (ΔG = −1.0 kcal/mol), in agreement with rapid disproportionation rates in water and organic solvents.[23] We hypothesized that the Cu^{I} complex could either react with an additional equivalent of hydrogen peroxide in a Fenton reaction or could react with O_2 produced from the disproportionation of either the hydroperoxyl radical or hydrogen peroxide. Experimentally, the reaction of the dibenzylamine containing parent ligand $L^{H,H}$, $[(L^{H,H})Cu^{I}]^{+}$ (**3**)[6] with dioxygen led to the formation of the bis-μ-oxo species $[\{(L^{H,H})Cu^{III}\}_2(\mu\text{-}O^{2-})_2]^{2+}$; however, no benzaldehyde was detected.[6] However, the addition of 5 or 10 equiv H_2O_2 to (**3**) in acetone at −80 °C leads to the formation of 35−45% benzaldehyde[17] indicating that the Cu^{I} intermediate was competent for amine oxidative N-dealkylation under the experimental conditions.

These results suggest that the reduced metal complex, formed after the homolysis of the Cu^{II}-OOH bond, undergoes a Fenton reaction with the pool of excess H_2O_2 (Scheme 12) present in solution, that was added for the initial synthesis/generation of the parent [(ligand)-Cu^{II}-OOH]$^{+}$ complex (*vide supra*). Electron transfer rates and calculations from Marcus theory disfavor an outer-sphere mechanism due to the unfavorable one electron reduction of hydrogen peroxide.[24] Instead, the proposed Fenton reaction would proceed via an inner sphere mechanism involving a Cu^{I}-OOH species. Presumably, this species is formed from a subsequent equivalent of hydrogen peroxide and involves a proton transfer to the excess triethylamine present in solution. DFT calculations suggest that the protonated triethylamine produced by this reaction prefers to form an explicit hydrogen bond with the proximal oxygen atom of the Cu^{I}-OOH species (Scheme 12), a process that is close to thermoneutral (ΔG = 1.1 kcal/mol). We also considered the formation of a Cu^{I}-OOH species where the protonated triethanol amine is hydrogen-bonded to the distal oxygen (Scheme 12); however, this species is predicted to be higher in energy (ΔG = 6.9 kcal/mol).

In iron-catalyzed Fenton chemistry, the oxidant responsible for C−H activation is believed to be either an iron^{IV}=O or a hydroxyl radical resulting from the homolysis or heterolysis of the O−O bond depending on the conditions of the reaction.[24,25] In the present system we computed the two analogous pathways, the formation of either a Cu^{II}-OH and $^{\bullet}$OH or a Cu^{II}-$O^{\bullet-}$ and H_2O (Scheme 12). The formation of a hydroxyl radical initially proceeds via a rapid proton transfer to the proximal oxygen (Scheme S10) to form a $Cu^{I}(H_2O_2)$ complex hydrogen-bonded to NEt_3 that is followed by homolysis of the O−O bond ($\Delta E^{\ddagger}$ = 2.4 kcal/mol and $\Delta G^{\ddagger}$ = 9.4 kcal/mol, Scheme 12 top). In contrast, the formation of a copper(II)-oxyl proceeds via a proton transfer to the distal oxygen and an intersystem crossing from the singlet Cu^{I}OOH species to the triplet Cu^{II}-$O^{\bullet-}$ species (Scheme 12 bottom). The barrier for this process can be approximated from the 2-D potential energy surface (Figures S17 and S18) and has a much larger barrier ($\Delta E_{ISC}^{\ddagger} \approx$ 12.9 kcal/mol) than the formation of a hydroxyl radical.

These results indicate that the formation of a hydroxyl radical is energetically more favorable than the formation of a Cu^{II}-$O^{\bullet-}$. The experimentally observed products would then result from a subsequent attack of the hydroxyl radical at the benzylic position of the ligand substrate producing a carbon radical that can then react with the Cu^{II}-OH moiety giving a ligand alcohol and copper(I) complex (Scheme 13). Under the strong overall oxidative conditions, the copper(I) ends up as copper(II) in the final product mixture (Scheme 13), as observed by EPR spectroscopy.

The possible presence of a hydroxyl radical under these conditions was experimentally evaluated with the oxygen-radical trap DMPO (5,5-dimethylpyrroline-*N*-oxide).[26,27] Addition of excess DMPO to the hydroperoxo solution (of $\mathbf{2}^{H,H}$) at −90 °C, dramatically decreases the yield of benzaldehyde (to

DOI: 10.1021/ja508371q
J. Am. Chem. Soc. 2015, 137, 2867−2874

Scheme 13

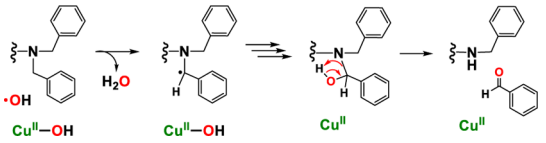

~20%) indicating that a radical species is responsible for the observed N-dealkylation products (Schemes 6 and 12). Also, EPR spectra (Figure S22) of the DMPO derivative radical are consistent with DMPO-OH,[27] the hydroxyl radical adduct of DMPO (see the Supporting Information for details). This result indicates that a hydroxyl radical is responsible for the observed C−H activation and is consistent with the site-specific Fenton reaction described here.

Overall, we propose a mechanism where the Cu^{II}-OOH species decays by rate determining Cu^{II}-OOH homolysis with a calculated barrier of $\Delta G^{\ddagger}$ = 14.3 kcal/mol, in agreement with the observed rate of Cu^{II}-OOH decay (4.17×10^{-2} s^{-1}). In a subsequent Fenton reaction, the Cu^{I} complex produced reacts with a second equivalent of hydrogen peroxide, which proceeds with a lower barrier ($\Delta G^{\ddagger}$ = 9.4 kcal/mol) (Scheme 12). Additionally, the absence of a product isotope effect in d_2-$L^{H,H}$ is consistent with the lack of an isotope effect observed in the reaction of a hydroxyl radical (generated from pulse radiolysis) with cyclohexane.[28]

These findings also lead us to warn researchers in copper or iron oxidative chemistries concerning the use of excess hydrogen peroxide (plus base) to generate M-($^{-}$OOH) complexes. Such procedures are very common,[6,10,11b,c,19b,29] but as seen here, the presence of additional H_2O_2 may complicate matters and allow for unintentional reaction pathways or mechanisms.

CONCLUSION

A mononuclear copper(II) hydroperoxide species possessing an appended dibenzylamine moiety is observed to be competent to perform the biomimetic (Scheme 1) oxidative N-dealkylation reaction to form benzaldehyde. A combination of experimental observations and DFT calculations indicates that the Cu^{II}-OOH species itself is *not* capable of performing C−H activation. This has led us to hypothesize and evaluate a new mechanism to account for the observed products involving rate-limiting Cu^{II}-OOH homolysis. The Cu^{I} species that is produced from this reaction further undergoes a Fenton reaction with an additional equivalent of H_2O_2. Experimental observations and DFT calculations favor homolytic O−O bond cleavage to form Cu^{II}-OH and $^{\bullet}$OH, where the hydroxyl radical is ultimately responsible for the C−H activation.

ASSOCIATED CONTENT

Supporting Information

Details concerning X-ray crystallographic analyses including cif files, EPR, UV−vis spectroscopies, cyclic voltammetry, ESI mass spectrometry, DFT calculations, and the procedures for carrying out the reactivity. This material is available free of charge via the Internet at http://pubs.acs.org.

AUTHOR INFORMATION

Corresponding Authors

*edward.solomon@stanford.edu
*karlin@jhu.edu

Author Contributions

§S.K. and J.W.G. contributed equally.

Notes

The authors declare no competing financial interest.

ACKNOWLEDGMENTS

The authors acknowledge support of this research from the National Institutes of Health (GM28962 from the National Institute of General Medical Sciences to K.D.K. and R01DK031450 from the National Institute of Diabetes and Digestive and Kidney Diseases to E.I.S.). The content is solely the responsibility of the authors and does not necessarily represent the official views of the National Institutes of Health.

REFERENCES

(1) (a) Itoh, S. *Curr. Opin. Chem. Biol.* **2006**, *10*, 115−122. (b) Mirica, L. M.; Ottenwaelder, X.; Stack, T. D. P. *Chem. Rev.* **2004**, *104*, 1013−1045. (c) Peterson, R. L.; Kim, S.; Karlin, K. D. In *Comprehensive Inorganic Chemistry II*, 2nd ed.); Oxford/Elsevier: Amsterdam, 2013; pp 149−177, http://dx.doi.org/10.1016/B978-0-08-097774-4.00309-0. (d) Peterson, R. L.; Ginsbach, J. W.; Cowley, R. E.; Qayyum, M. F.; Himes, R. A.; Siegler, M. A.; Moore, C. D.; Hedman, B.; Hodgson, K. O.; Fukuzumi, S.; Solomon, E. I.; Karlin, K. D. *J. Am. Chem. Soc.* **2013**, *135*, 16454−16467.

(2) (a) Klinman, J. P. *Chem. Rev.* **1996**, *96*, 2541−2561. (b) Klinman, J. P. *J. Biol. Chem.* **2006**, *281*, 3013−3016. (c) Prigge, S. T.; Eipper, B.; Mains, R.; Amzel, L. M. *Science* **2004**, *304*, 864−867. (d) Solomon, E. I.; Heppner, D. E.; Johnston, E. M.; Ginsbach, J. W.; Cirera, J.; Qayyum, M.; Kieber-Emmons, M. T.; Kjaergaard, C. H.; Hadt, R. G.; Tian, L. *Chem. Rev.* **2014**, *114*, 3659−3853.

(3) (a) Evans, J. P.; Ahn, K.; Klinman, J. P. *J. Biol. Chem.* **2003**, *278*, 49691−49698. (b) Bauman, A. T.; Yukl, E. T.; Alkevich, K.; McCormack, A. L.; Blackburn, N. J. *J. Biol. Chem.* **2006**, *281*, 4190−4198.

(4) Chen, P.; Bell, J.; Eipper, B. A.; Solomon, E. I. *Biochemistry* **2004**, *43*, 5735−5747.

(5) (a) Chen, P.; Solomon, E. I. *J. Am. Chem. Soc.* **2004**, *126*, 4991−5000. (b) Cramer, C.; Tolman, W. *Acc. Chem. Res.* **2007**, *40*, 601−608.

(6) Maiti, D.; Narducci Sarjeant, A. A.; Karlin, K. D. *Inorg. Chem.* **2008**, *47*, 8736−8747.

(7) Maiti, D.; Lee, D.-H.; Gaoutchenova, K.; Würtele, C.; Holthausen, M. C.; Sarjeant, A. A. N.; Sundermeyer, J.; Schindler, S.; Karlin, K. D. *Angew. Chem. Int. Ed.* **2008**, *47*, 82−85.

(8) (a) Comba, P.; Knoppe, S.; Martin, B.; Rajaraman, G.; Rolli, C.; Shapiro, B.; Stork, T. *Chem.—Eur. J.* **2008**, *14*, 344−357. (b) Himes, R. A.; Karlin, K. D. *Curr. Opin. Chem. Biol.* **2009**, *13*, 119−131. (c) Decker, A.; Solomon, E. I. *Curr. Opin. Chem. Biol.* **2005**, *9*, 152−163. (d) Yoshizawa, K.; Kihara, N.; Kamachi, T.; Shiota, Y. *Inorg. Chem.* **2006**, *45*, 3034−3041. (e) Crespo, A.; Marti, M. A.; Roitberg, A. E.; Amzel, L. M.; Estrin, D. A. *J. Am. Chem. Soc.* **2006**, *128*, 12817−12828. (f) Huber, S. M.; Ertem, M. Z.; Aquilante, F.; Gagliardi, L.; Tolman, W. B.; Cramer, C. J. *Chem.—Eur. J.* **2009**, *15*, 4886−4895.

(9) (a) Peterson, R. L.; Himes, R. A.; Kotani, H.; Suenobu, T.; Tian, L.; Siegler, M. A.; Solomon, E. I.; Fukuzumi, S.; Karlin, K. D. *J. Am. Chem. Soc.* **2011**, *133*, 1702−1705. (b) Ginsbach, J. W.; Peterson, R. L.; Cowley, R. E.; Karlin, K. D.; Solomon, E. I. *Inorg. Chem.* **2013**, *52*, 12872−12874. (c) Woertink, J. S.; Tian, L.; Maiti, D.; Lucas, H. R.; Himes, R. A.; Karlin, K. D.; Neese, F.; Würtele, C.; Holthausen, M. C.; Bill, E.; Sundermeyer, J.; Schindler, S.; Solomon, E. I. *Inorg. Chem.* **2010**, *49*, 9450−9459.

(10) (a) Maiti, D.; Narducci Sarjeant, A. A.; Karlin, K. D. *J. Am. Chem. Soc.* **2007**, *129*, 6720−6721. (b) Kim, S.; Saracini, C.; Siegler, M. A.; Drichko, N.; Karlin, K. D. *Inorg. Chem.* **2012**, *51*, 12603−12605.

(11) (a) Wada, A.; Harata, M.; Hasegawa, K.; Jitsukawa, K.; Masuda, H.; Mukai, M.; Kitagawa, T.; Einaga, H. *Angew. Chem., Int. Ed.* **1998**, *37*, 798−799. (b) Yamaguchi, S.; Masuda, H. *Sci. Technol. Adv. Mater.*

DOI: 10.1021/ja508371q
J. Am. Chem. Soc. 2015, 137, 2867−2874

2005, *6*, 34−47. (c) Kunishita, A.; Kubo, M.; Ishimaru, H.; Ogura, T.; Sugimoto, H.; Itoh, S. *Inorg. Chem.* **2008**, *47*, 12032−12039.
(12) Thierbach, D.; Huber, F.; Preut, H. *Acta Crystallogr.* **1980**, *B36*, 974−977.
(13) (a) Mure, M.; Klinman, J. P. *J. Am. Chem. Soc.* **1995**, *117*, 8707−8718. (b) Chen, Y. K.; Jeon, S. J.; Walsh, P. J.; Nugent, W. A. *Org. Synth.* **2005**, *82*, 87−92.
(14) Frisch, M. J., et al. *Gaussian 09*; Gaussian, Inc.: Wallingford, CT, 2009. (For the full reference, see the Supporting Information.)
(15) Poater, A.; Cavallo, L. *Inorg. Chem.* **2009**, *48*, 4062−4066.
(16) Frisch, M. J., et al. *Gaussian 03*; Gaussian, Inc.: Wallingford, CT, 2004. (For the full reference, see the Supporting Information.)
(17) See Supporting Information.
(18) (a) Lam, W. W. Y.; Yiu, S. M.; Yiu, D. T. Y.; Lau, T. C.; Yip, W. P.; Che, C. M. *Inorg. Chem.* **2003**, *42*, 8011−8018. (b) Kunishita, A.; Kubo, M.; Sugimoto, H.; Ogura, T.; Sato, K.; Takui, T.; Itoh, S. *J. Am. Chem. Soc.* **2009**, *131*, 2788−2789.
(19) (a) Kamachi, T.; Lee, Y.-M.; Nishimi, T.; Cho, J.; Yoshizawa, K.; Nam, W. *J. Phys. Chem. A* **2008**, *112*, 13102−13108. (b) Choi, Y. J.; Cho, K.-B.; Kubo, M.; Ogura, T.; Karlin, K. D.; Cho, J.; Nam, W. *Dalton T* **2011**, *40*, 2234−2241.
(20) Lin, T.-Y.; Wu, C.-H. *J. Catal.* **2005**, *232*, 117−126.
(21) (a) Karlin, K. D.; Haka, M. S.; Cruse, R. W.; Gultneh, Y. *J. Am. Chem. Soc.* **1985**, *107*, 5828−5829. (b) Lucas, H. R.; Karlin, K. D. *Met. Ions Life Sci.* **2009**, *6*, 295−361. (c) Lucas, H. R.; Meyer, G. J.; Karlin, K. D. *J. Am. Chem. Soc.* **2010**, *132*, 12927−12940.
(22) *Handbook of Bond Dissociation Energies in Organic Compounds*; Luo, Y.-R., Ed.; CRC: Boca Raton, FL, 2003.
(23) (a) Bielski, B. H. J.; Allen, A. O. *J. Phys. Chem.* **1977**, *81*, 1048−1050. (b) Chin, D. H.; Chiericato, G.; Nanni, E. J.; Sawyer, D. T. *J. Am. Chem. Soc.* **1982**, *104*, 1296−1299.
(24) Goldstein, S.; Meyerstein, D.; Czapski, G. *Free Radic. Biol. Med.* **1993**, *15*, 435−445.
(25) (a) Groves, J. T.; McClusky, G. A. *J. Am. Chem. Soc.* **1976**, *98*, 859−861. (b) Dunford, H. B. *Coord. Chem. Rev.* **2002**, *233*−*234*, 311−318. (c) Pestovsky, O.; Stoian, S.; Bominaar, E. L.; Shan, X.; Munck, E.; Que, L.; Bakac, A. *Angew. Chem., Int. Ed.* **2005**, *44*, 6871−6874.
(26) (a) Hetterscheid, D. G. H.; Bens, M.; de Bruin, B. *Dalton Trans.* **2005**, 979−984. (b) Li, L. X.; Abe, Y.; Kanagawa, K.; Usui, N.; Imai, K.; Mashino, T.; Mochizuki, M.; Miyata, N. *Anal. Chim. Acta* **2004**, *512*, 121−124.
(27) (a) Buettner, G. R. *Free Radic. Biol. Med.* **1987**, *3*, 259−303. (b) Hanna, P. M.; Chamulitrat, W.; Mason, R. P. *Arch. Biochem. Biophys.* **1992**, *296*, 640−644. (c) Chignell, C. F.; Motten, A. G.; Sik, R. H.; Parker, C. E.; Reszka, K. *Photochem. Photobiol.* **1994**, *59*, 5−11. (d) Althoff, F.; Benzing, K.; Comba, P.; McRoberts, C.; Boyd, D. R.; Greiner, S.; Keppler, F. *Nat. Commun.* **2014**, *5*, No. 4205. (e) EPR Detection of the Superoxide Free Radical with the Nitrone Spin Traps DMPO and BMPO, https://http://www.bruker.com/fileadmin/user_upload/8-PDF-Docs/MagneticResonance/EPR_brochures/superoxide.pdf. (f) We attribute the detection of only DMPO-OH, and not DMPO-OOH, to two factors. First, the trapping $HOO^{\bullet}$ radical by DMPO is a very slow reaction while the reaction of DMPO and $HO^{\bullet}$ is very fast. Second, DMPO-OOH is quite unstable and spontaneously decays to the DMPO-OH adduct ($t_{1/2}$ = 45 s). Thus, we really cannot observe/detect DMPO-OOH under our experimental conditions. See SI for references..
(28) Buxton, G. V.; Greenstock, C. L.; Helman, W. P.; Ross, A. B. *J. Phys. Chem. Ref. Data* **1988**, *17*, 513−886.
(29) (a) Yamaguchi, S.; Nagatomo, S.; Kitagawa, T.; Funahashi, Y.; Ozawa, T.; Jitsukawa, K.; Masuda, H. *Inorg. Chem.* **2003**, *42*, 6968−6970. (b) Yamaguchi, S.; Kumagai, A.; Nagatomo, S.; Kitagawa, T.; Funahashi, Y.; Ozawa, T.; Jitsukawa, K.; Masuda, H. *Bull. Chem. Soc. Jpn.* **2005**, *78*, 116−124. (c) Yamaguchi, S.; Wada, A.; Nagatomo, S.; Kitagawa, T.; Jitsukawa, K.; Masuda, H. *Chem. Lett.* **2004**, *33*, 1556−1557. (d) Itoh, K.; Hayashi, H.; Furutachi, H.; Matsumoto, T.; Nagatomo, S.; Tosha, T.; Terada, S.; Fujinami, S.; Suzuki, M.; Kitagawa, T. *J. Am. Chem. Soc.* **2005**, *127*, 5212−5223. (e) Kunishita, A.; Scanlon, J. D.; Ishimaru, H.; Honda, K.; Ogura, T.; Suzuki, M.; Cramer, C. J.; Itoh, S. *Inorg. Chem.* **2008**, *47*, 8222−8232. (f) Maiti, D.; Lucas, H. R.; Sarjeant, A. A. N.; Karlin, K. D. *J. Am. Chem. Soc.* **2007**, *129*, 6998−6999. (g) Burg, A.; Shusterman, I.; Kornweitz, H.; Meyerstein, D. *Dalton Trans.* **2014**, *43*, 9111−9115. (h) Kim, D.; Cho, J.; Lee, Y. M.; Sarangi, R.; Nam, W. *Chem.—Eur. J.* **2013**, *19*, 14112−14118. (i) Guzei, I. A.; Bakac, A. *Inorg. Chem.* **2001**, *40*, 2390−2393. (j) Song, W.; Bakac, A. *Inorg. Chem.* **2010**, *49*, 150−156. (k) Martinho, M.; Blain, G.; Banse, F. *Dalton Trans.* **2010**, *39*, 1630−1634.

DOI: 10.1021/ja508371q
J. Am. Chem. Soc. 2015, 137, 2867−2874